IEEE Access
Multidisciplinary ⋮ Rapid Review ⋮ Open Access Journal

Received March 9, 2021, accepted March 27, 2021, date of publication April 5, 2021, date of current version April 19, 2021.

Digital Object Identifier 10.1109/ACCESS.2021.3070864

Integrated Control Strategy for Electrolytic Aluminum Load Participation in Frequency Modulation

XIN SHEN[1,2,3], (Member, IEEE), HONGCHUN SHU[1], (Member, IEEE), ZHENGYUN FAN[2], AND XI MO[3]

[1]Faculty of Electric Power Engineering, Kunming University of Science and Technology, Kunming 650500, China
[2]Yunnan Power Grid Company Ltd., Kunming 650011, China
[3]Yunnan Electric Power Dispatching and Control Center, Kunming 650000, China

Corresponding author: Xin Shen (shenxin@stu.kust.edu.cn)

This work was supported in part by the National Natural Science Foundation of China under Grant 52037003 and Grant 51977102, and in part by the Key Science and Technology Project of Yunnan Province under Grant 202002AF080001.

ABSTRACT The introduction of electrolytic aluminum load in a large-scale power system with complex power station structure is essential for load frequency control (LFC). In this paper, we propose a control strategy for electrolytic aluminum load to participate in the frequency modulation of the power grid based on the IEEE standard two-region LFC model. Besides, a fractional-order PID (FOPID) controller is designed and compared with traditional PID, and the parameters of the FOPID controller are optimized by PSO algorithm. In addition, a two-region LFC model was built to verify the integrated control strategy for electrolytic aluminum load participation in frequency modulation, which show that the FOPID controller optimized by the PSO algorithm has stronger robustness in the LFC.

INDEX TERMS Electrolytic aluminum, LFC, FOPID, integrated control strategy.

NOMENCLATURE

A. SETS

LFC	Load frequency control
FOPID	Fractional-order proportional integral derivative control
PID	Proportional integral derivative control
AGC	Automatic power generation control system
FTC	Flat tie-line control
FFC	Flat frequency control
TBC	Tie -line load frequency bias control
ACE	Area control error

B. PARAMETERS

Δf	System frequency deviation
ΔP_{tie}	Exchange power deviation of the tie line
$K\tau$	Ratio of the power generated by steam in the high pressure cylinder section to the total power of the steam turbine
$T\tau$	Reheater time constant
τ_T	Steam chamber time constant and the main inlet volume
T_g	Time constant of the governor
M	Unit inertia constant
D	System load damping constant
E_i, E_j	Voltages across the tie line of the corresponding area
θ_i, θ_j	Power angles corresponding to the area i and area j
X_{ij}	Equivalent reactance of the tie line
θ_{i0}, θ_{j0}	Initial power angle
Δf_i, Δf_j	Frequency change values of regions i and j, respectively
T_{ij}	Synchronization coefficient of the tie line
$\Delta\theta_i$, $\Delta\theta_j$	The changes in the power angle of the corresponding area
$\Delta P_{Alref}(S)$	Control signal of the electrolytic aluminum load
$\Delta P_{Al}(S)$	Actual adjustment change of the electrolytic furnace load, and a and b are the equivalent parameters of the electrolytic aluminum load dynamic response model
a, t	Upper and lower limits of differentiation or integration, and α is the order of calculus
α	Fractional differential order
s	Adjustable parameters

The associate editor coordinating the review of this manuscript and approving it for publication was Eklas Hossain.

R	Resistance
E	A back electromotive force
V_{AH}	High-voltage side voltage of the load bus
α	The order and can take any real number
n	Integer
ω_b, ω_h	Approximate frequency band
Δf_i, Δf_j	Frequency change values of regions i and j, respectively
V_{AL}	Low-voltage side voltage of the load bus
k	Transformation ratio of the aluminum plant transformer
I_d	Electrolytic cell current
P_{ASL}	Electrolytic aluminum load power
$\dot{\boldsymbol{P}}_{ASL}$	The derivative of electrolytic aluminum load power
ΔP_{ASLref}	Electrolytic aluminum load power value
L_{sr}	Inductance value of the saturated reactor
V_B	DC voltage
F_{ref}	Rated frequency of the system
Δf	Change in frequency in the system
ΔP	Change in power of the electrolytic aluminum load participating in frequency control
K_s	Unit regulated power of the electrolytic aluminum load
M_E	Inertia control coefficient

I. INTRODUCTION

The reliability of power system operation and control has been widely challenged by the persistent proliferation of high energy consumption in various regions of the world [1]–[3]. It is important to explore large-scale and rapid adjustment resources to improve power system flexibility. To this end, researchers explore the frequency modulation potential of high-energy-consuming electrolytic aluminum loads.

Recently, the random volatility of renewable energy power generation places increasingly severe pressure on the safe power grid operation. The large-scale energy storage available in support components can significantly improve the power grid flexibility and increase power consumption capacity. However, energy storage batteries are expensive and have high capacity. Furthermore, it is difficult to select pumped storage power station sites. It is not realistic to solve large-scale new energy consumption problems entirely through energy storage. The demonstration applications on the demand side are limited to residential areas. High energy-consuming industrial loads have large installed capacities, centralized control, and low transformation costs, and they have considerable potential for regulation. High energy-consuming loads, such as electrolytic aluminum and hydroelectric silicon, are thermal energy storage loads with large thermal inertia. Short-term adjustment has little effect on normal load production and is suitable for rapid power system dynamic adjustments.

Energy storage and demand-side response are combined to coordinate and control the transmission power of the high-penetration microgrid and the large-scale grid tie line. The [4] verifies the load-side response through theoretical derivation, which is conducive to improving the frequency dynamic response of the power system and enhancing the stability of the system. Reference [5] proposed the use of air-conditioning load to stabilize the power meter fluctuation of the power grid connection line, and [6] proposed using the cluster energy storage characteristics of electric vehicles to study the strategy of clustering electric vehicles to stabilize the power fluctuation of the connection line. Reference [7] proposes a distributed direct load control method, which realizes the aggregation of large-scale residential commercial loads and increases the scale of equivalent energy storage for residential and commercial loads. Some papers focuses on the participation of residential and commercial loads in power grid frequency regulation, and only few of them study on industrial loads participating in power grid frequency regulation. Reference [8] proposes to use the control strategy of cement plant start-stop control and energy storage coordination to participate in grid frequency modulation, due to the limitations of energy storage devices, the scalability of this method is limited. The [9]–[12] analyzes the adjustment ability of electrolytic aluminum load, and can adjust the electrolytic aluminum load power by adjusting the excitation voltage and other methods. In order to improve dynamic performance of frequency control in the isolated system, the [13] proposes an MPC-based frequency controller to keep the frequency deviation within a proper range under wind power fluctuation as well as to recover the system frequency under some large disturbance.

The paper propose a control strategy for electrolytic aluminum load to participate in the frequency modulation of the power grid based on the IEEE standard two-region load frequency control model.

The contributions of this paper are listed as follows:

(1) A fractional-order PID controller was designed to enhance the robustness of the control system while electrolytic aluminum load connected in frequency modulation, and the specific parameters of this controller were optimized by PSO algorithm.

(2) A integrated control strategy is proposed by combining the droop control and virtual inertia control characteristics to enhance the LFC performance of the electrolytic aluminum load.

(3) Different frequency control result was obtained considering the different demand response and random disturbance in the simulation.

The remainder of this paper is organized as follows. A fractional-order PID controller was designed to ensure the electrolytic aluminum load control performance in section II. A second-order transfer model is introduced to approximate the actual output of electrolytic aluminum load in section III. Electrolytic aluminum loading control strategy is proposed by combining the droop control and virtual inertia

control characteristics in section V. Section VI concludes this paper.

II. SYSTEM MODEL

A. AUTOMATIC GENERATION CONTROL

AGC is currently the most widely used secondary frequency modulation methods. The AGC changes the control area unit output by receiving such information as system frequency deviation and tie line power deviation. There are three primary AGC control mode types: flat tie-line control (FTC), flat frequency control (FFC), and tie line power and frequency deviation control (TBC). These three modes introduce the area control error (ACE) to describe the imbalance between the load demand and the generator set active power output. The TBC control mode is generally selected for multi-region interconnected systems shown as (1),

$$ACE = \Delta P_{tie} + \beta \Delta f \tag{1}$$

B. LOAD FREQUENCY CONTROL UNIT MODEL

1) CREW MODEL

In this study, the reheated steam turbine was used as the prime mover for analysis. The transfer function model can be expressed as (2),

$$Gen(s) = \frac{1}{1+\tau_T s} \cdot \frac{1+K_\tau T_\tau s}{T_\tau s+1} \tag{2}$$

2) GOVERNOR MODEL

The turbine governor transfer function model can be described as (3),

$$Gov(s) = \frac{1}{T_g s+1} \tag{3}$$

3) GENERATOR-POWER SYSTEM MODEL

The generator power system transfer function model can be described as (4),

$$Gor(s) = \frac{1}{Ms+D} \tag{4}$$

4) TIE LINE MODEL

The per transmission power between two interconnected regions can be written as (5),

$$P_{ij} = \frac{|E_i|\,|E_j|}{X_{ij}} \sin(\theta_i - \theta_j) \tag{5}$$

When the power angle changes, the transmission power of the two regions is shown as (6),

$$P_{ij} = \frac{|E_i|\,|E_j|}{X_{ij}} \cos(\theta_{i0} - \theta_{j0})(\Delta\theta_i - \Delta\theta_j) \tag{6}$$

The tie line power increment model can be described as (7),

$$P_{ij} = \frac{|E_i|\,|E_j|}{X_{ij}} \cos(\theta_{i0} - \theta_{j0})\left(\int \Delta f_i dt - \int \Delta f_j dt\right) \tag{7}$$

After the Lass transform, the tie line transfer function model can be described as (8),

$$\Delta P_{ij}(s) = \frac{T_{ij}}{s}\left[\Delta f_i(s) - \Delta f_j(s)\right] \tag{8}$$

C. FRACTIONAL-ORDER PROPORTIONAL INTEGRAL DERIVATIVE CONTROL

1) FRACTIONAL CALCULUS DEFINITION

The fractional calculus operator is usually defined in a piecewise function as (9),

$${}_aD_t^\alpha = \begin{cases} \dfrac{\mathrm{d}^\alpha}{\mathrm{d}t^\alpha}, & \alpha > 0 \\ 1, & \alpha = 0 \\ \int_a^t (\mathrm{d}\tau)^{-\alpha}, & \alpha < 0 \end{cases} \tag{9}$$

There are three common fractional calculus definitions:

1) Grunwald-Letnikov's is defined as (10),

$${}_aD_t^\alpha f(t) = \lim_{h\to 0} \frac{1}{h^\alpha} \sum_{j=0}^{[(t-a/h)]} (-1)^j f(t-jh) \frac{\alpha!}{j!(\alpha-j)!} \tag{10}$$

2) Riemann-Liouville's is defined as (11),

$${}_aD_t^\alpha f(t) = \frac{1}{\Gamma(m-\alpha)} \left(\frac{\mathrm{d}}{\mathrm{d}t}\right)^m \int_a^t \frac{f(\tau)}{(t-\tau)^{1-(m-\alpha)}} d\tau \tag{11}$$

where $m\text{-}1 \leq \alpha \leq m$, and $\Gamma(x)$ is the Gamma function.

3) Caputo's is defined as (12),

$${}_aD_t^\alpha f(t) = {}_aI_t^{n-\alpha} D^n f(t) = \frac{1}{\Gamma(n-\alpha)} \int_a^t \frac{f^{(n)}(\tau)}{(1-\tau)^{\alpha-n+1}} d\tau \tag{12}$$

2) FRACTIONAL ORDER CONTROLLER

The traditional PID controller mentioned above is fractional-order. FIGURE 1 shows the fractional-order PIλDμ control system functional block diagram:

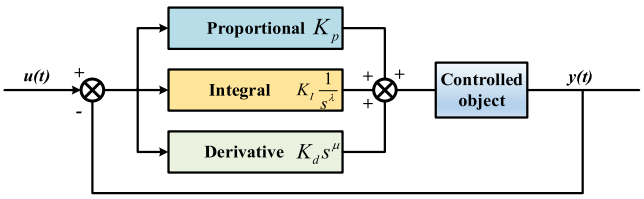

FIGURE 1. FOPID controller.

The fractional-order $PI^\lambda D^\mu$ controller adds two parameters λ and μ to the traditional PID controller. the resulting transfer function expression can be written as (13),

$$C(s) = K_p + K_i s^{-\lambda} + K_D s^\mu \tag{13}$$

When λ and μ both set as 1, the fractional-order $PI^\lambda D^\mu$ controller is the traditional PID controller,

3) FRACTIONAL PID ADVANTAGES

Adding parameters λ and μ make the fractional-order $PI^{\lambda}D^{\mu}$ controller more flexible. The range of λ and μ values changes from the original three points to a single plane, and the adjustment range increases significantly. In traditional PID control phase adjustment, the integral link lags the phase by 90° to eliminate the steady-state error, while the differential link advances the phase by 90° to improve the system dynamic performance. However, the fixed addition and subtraction of 90° may hamper efforts to achieve the best control effect. The first-order $PI^{\lambda}D^{\mu}$ controller can achieve any angle adjustment between 0 and 180° in advance or lag. Moreover, the $PI^{\lambda}D^{\mu}$ controller integral link is not only related to the current moment, the $PI^{\lambda}D^{\mu}$ controller integral and differential links are related to all historical moment values, and they have memory.

4) IMPROVED OUSTALOUP INDIRECT APPROXIMATION ALGORITHM

The Oustaloup algorithm is a widely used indirect approximation algorithm. It shows good approximation performance in terms of amplitude and phase frequency characteristics, but its approximation effect near the end of the frequency band is poor. Therefore, we improved the Oustaloup indirect approximation algorithm by adding a filter to approximate the frequency band and at the endpoint.

By selecting the approximate frequency band $[\omega_b, \omega_h]$, the fractional differential operator s^{α} in the frequency band can be approximated as a transfer function $K(s)$, which can be shown as (14),

$$K(s)=\left(\frac{1+\frac{s}{d\omega_b/b}}{1+\frac{s}{b\omega_h/d}}\right)^{\alpha}=\left(\frac{bs}{d\omega_b}\right)^{\alpha}\left(1+\frac{-ds^2+d}{ds^2+b\omega_h s}\right)^{\alpha} \tag{14}$$

where $0<\alpha<1$, α is the fractional differential order; and $s=j\omega$; $b>0$, $d>0$, which are adjustable parameters. Introducing the two coefficients b and d improves the effect at both ends of the approximate frequency band. The frequency band $\omega_b<\omega<\omega_h$ is expanded by the Taylor power series and obtained by taking the first-order approximation as (15),

$$K(s)=(\frac{bs}{d\omega_b})^{\alpha}[1+\alpha p(s)+\frac{\alpha(\alpha-1)}{2}p^2(s)+\cdots] \tag{15}$$

$p(s)$ is defined as (16),

$$p(s)=\frac{-ds^2+d}{ds^2+b\omega_h s} \tag{16}$$

Omitting the higher-order terms in the Taylor expansion, (15) can be shown as (17),

$$s^{\alpha}\approx\left(\frac{d\omega_b}{b}\right)^{\alpha}\left(\frac{ds^2+b\omega_h s}{d(1-\alpha)s^2+b\omega_h s+d\alpha}\right)\left(\frac{1+\frac{s}{d\omega_b/b}}{1+\frac{s}{b\omega_h/d}}\right)^{\alpha} \tag{17}$$

where $0<\alpha<1, b>0, d>0$, and the Oustaloup filter is used to expand the last item in(17), which can be shown as (18),

$$s^{\alpha}\approx\left(\frac{d\omega_b}{b}\right)^{\alpha}\left(\frac{ds^2+b\omega_h s}{d(1-\alpha)s^2+b\omega_h s+d\alpha}\right)\prod_{k=-N}^{N}\frac{s+\omega_k'}{s+\omega_k} \tag{18}$$

There are $2N+1$ zeros and poles. The k-th real zeros and poles can be written as (19),

$$\omega_k'=(\frac{d\omega_b}{b})^{\frac{\alpha-2k}{2N+1}},\quad \omega_k=(\frac{b\omega_h}{d})^{\frac{\alpha+2k}{2N+1}} \tag{19}$$

Then, the final continuous rational transfer function model is obtained as (20),

$$K(s)\approx(\frac{d\omega_b}{b})^{\alpha}[\frac{ds^2+b\omega_h s}{d(1-\alpha)s^2+b\omega_h s+d\alpha}]\prod_{k=-N}^{N}\frac{s+\omega_k'}{s+\omega_k} \tag{20}$$

The Oustaloup approximation algorithm is used in [14]. The values of b and d directly affect the approximation accuracy, and the approximation effect is better when $b=10$ and $d=9$. The research frequency band continues to use $[10^{-3}, 10^{3}]$.

III. ELECTROLYTIC ALUMINUM LOAD MODEL

A. ELECTROLYTIC ALUMINUM LOAD VOLTAGE-POWER MODEL

The electrolytic aluminum load cell can be equivalent to the circuit shown in FIGURE 2 with a combination of resistance R and a back electromotive force E. R is the electrolytic cell equivalent resistance, V_{AH} is the high-voltage side of the load bus, V_{AL} is the low-voltage side of the load bus, k is the transformation ratio of the aluminum plant transformer, and LSR is the saturated reactor inductance value.

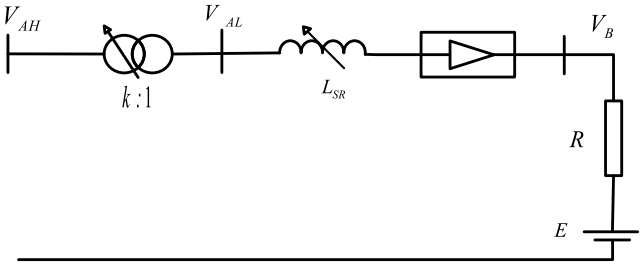

FIGURE 2. Electrolytic aluminum load equivalent circuit diagram.

Relevant data were obtained through field tests [17], and the least square method was used to fit the electrolytic aluminum load equivalent model parameters. The equivalent resistance R was 2.016 mΩ, and the electromotive force E was 354.6.

The electrolytic aluminum load cell DC bus voltage drop can be expressed as (21),

$$V_B=I_dR+E \tag{21}$$

R and E are related to the cell electrolyte composition, temperature, and electrode distance. In general, R and E are regarded as constants.

Therefore, the electrolytic aluminum load active power P_{ASL} can be expressed as (22),

$$P_{ASL} = V_B I_B = \frac{V_B (V_B - E)}{R} = \frac{V_B (V_B - 354.6)}{2.016} \times 10^{-3} (MW) \quad (22)$$

The (22) shows that the electrolytic aluminum load active power can be controlled by controlling the DC voltage V_B.

B. ELECTROLYTIC ALUMINUM LOAD REGULATION METHOD

The electrolytic aluminum load active power can be controlled by controlling the voltage on the DC side of the electrolytic aluminum load. Figure 2 shows that the active power can be controlled by adjusting the saturated reactor and the high voltage side.

1) SATURATED REACTOR CONTROL

By adjusting the control winding current I_c, the initial iron core magnetic density can be changed, the commutation time can be changed, the output current can be controlled, and the electrolytic aluminum active power can be adjusted.

Based on the electrolytic aluminum load steady flow control system, the corresponding experimental data were obtained by superimposing the negative step signal [13], and the experimental data were fitted by the least square method. The result was expressed as (23),

$$P(t) = 0.165 \times e^{-0.502t} - 0.056 \times e^{-1.994t} + 0.8883 \quad (23)$$

Rewritten into a transfer function, (23) was expressed as (24),

$$G_{ASL}(s) = \frac{Y(s)}{U(s)} = \frac{\Delta P_{ASL}(s)}{\Delta P_{ASLref}(s)} = \frac{1}{s^2 + 2.496s + 1} \quad (24)$$

The state equation was expressed as (25),

$$\begin{bmatrix} \Delta \dot{P}_{ASL} \\ \Delta \ddot{P}_{ASL} \end{bmatrix} = \begin{bmatrix} 0 & 1 \\ -1 & -2.496 \end{bmatrix} \begin{bmatrix} \Delta P_{ASL} \\ \Delta \dot{P}_{ASL} \end{bmatrix} + \begin{bmatrix} 0 \\ 1 \end{bmatrix} \Delta P_{ASLref} \quad (25)$$

The fitted curve was consistent with the experimental data, which can be used to approximate the electrolytic aluminum power adjustment process.

2) HIGH VOLTAGE SIDE REGULATION CONTROL

As (22) shows that the electrolytic aluminum load active power can be adjusted by controlling the DC voltage V_B. The relationship between the DC voltage V_B and the high-voltage side bus voltage V_{AH} is shown in the following (26),

$$V_B = \frac{\left(\frac{1.35 V_{AH}}{k} + \frac{3\omega}{2\pi} \frac{L_{SR} E}{R}\right)}{\left(1 + \frac{3\omega}{2\pi} \frac{L_{SR}}{R}\right)} \quad (26)$$

Since the change in ω is small, it can be regarded as a constant, and the inductance value L_{SR} of the saturated reactor is also constant. The equivalent resistance R and E are only related to the electrolyte composition, the electrolytic cell temperature and the distance between the electrodes; therefore, they can be regarded as constants.

Therefore, the (26) can be approximately expressed as (27),

$$V_B = \frac{2.7\pi R}{2k\pi R + 3\omega L_{SR}} V_{AH} = K_{AH} V_{AH} \quad (27)$$

The DC voltage VB variation can be expressed as (28),

$$\Delta V_B = K_{AH} \Delta V_{AH} \quad (28)$$

The (22) shows when the DC voltage is changed, the electrolytic aluminum load active power is expressed as (29),

$$P'_{ASL} = (V_B + \Delta V_B) I_B = \frac{(V_B + \Delta V_B)((V_B + \Delta V_B) - E)}{R} = \frac{(V_B + \Delta V_B)((V_B + \Delta V_B) - 354.6)}{2.016} \times 10^{-3} (MW) \quad (29)$$

The incremental value of active power can be expressed as follows (30),

$$\Delta P_{ASL} = P'_{ASL} - P_{ASL} = K_1 \Delta V_B = K_1 K_{AH} V_{AH} \quad (30)$$

The (30) show that the electrolytic aluminum load active power can be controlled by adjusting the high side voltage V_{AH}.

Based on the field test results [13], the applied step signal was used to test the change in the relationship between the electrolytic aluminum load active power and the generator terminal voltage, and the field data were fitted by the least square method. The result is expressed as (31),

$$\Delta P_{SAL}(t) = -0.054 + 0.054 e^{-2.782t} \quad (31)$$

The transfer function of (31) was obtained as (32),

$$G_{ASL}(s) = \frac{Y(s)}{U(s)} = \frac{\Delta P_{ASL}(s)}{\Delta V_G(s)} = \frac{0.054}{s + 2.782} \quad (32)$$

IV. ELECTROLYTIC ALUMINUM LOAD PARTICIPATES IN A TWO-ZONE FREQUENCY CONTROL STRATEGY

A high-energy-consuming electrolytic aluminum load has a fast and accurate response capability and high economy. Because the high energy consuming electrolytic aluminum load has a large thermal energy storage inertia, short-term consumption adjustments do not affect the product quality. Therefore, the load participates in the power grid frequency modulation, which charges the electrolytic aluminum load frequency modulation potential and effectively improves the power grid frequency fluctuation.

When the electrolytic aluminum load participates in power grid frequency regulation, the load characteristics need to be considered. Since the electrolytic aluminum load is an important first-order load, a constant DC power supply must be ensured. Large fluctuations affect the electrolytic cell thermal stability, resulting in an internal heat imbalance in the cell

and introduces production problems. Therefore, the safe and adjustable electrolytic aluminum load capacity is 10% of its rated capacity; in other words, electrolytic aluminum has a continuous adjustment capacity of 90-110%. In this range, electrolytic aluminum production is not affected, but rather only shifts one equilibrium point to another. For this reason, a corresponding limiter must be designed to limit the electrolytic aluminum load output. Dead zone adjustments are required to avoid frequent start-up. For off-grid high-energy-consuming industrial power grids, the allowable system frequency deviation range is 0.2 Hz; therefore, the electrolytic aluminum load control dead zone is set to 0.2 Hz, which effectively avoids frequent starts and affects production. When the system frequency exceeds the range, the electrolytic aluminum load participates in the grid frequency modulation in time. FIGURE 3 shows the load model diagram considering the electrolytic aluminum load characteristics.

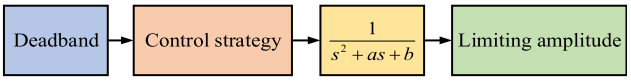

FIGURE 3. Simulation model considering the electrolytic aluminum load characteristics.

When the grid frequency deviation is large, the electrolytic aluminum load may participate in the grid frequency adjustment control; in other words, the electrolytic aluminum load adjusts the load according to the size of the grid frequency difference to improve the grid frequency. Conventional power supply frequency modulation is limited to the unit side, slowing the response speed and making it difficult to meet the frequency modulation requirements. Since primary frequency modulation is a minute-level method, the electrolytic aluminum load may be adjusted to the response load to participate in the grid system secondary frequency modulation.

A. DROOP CONTROL

In the power system, the relationship between the system load active power and the frequency change is the static frequency characteristic. Therefore, the electrolytic aluminum load droop control participating in the power system frequency modulation was defined as (33),

$$\Delta P = K_s \left(f - f_{ref}\right) = K_s \cdot \Delta f \tag{33}$$

When the system frequency changes, the droop control module will adjust the adjustable operating power of the electrolytic aluminum load in a certain proportion according to the frequency change.

B. VIRTUAL INERTIA CONTROL

The virtual inertia control mechanism simulates the inertia corresponding traditional generator set links, adjust active power according to the frequency rate of change, release or absorb rotor kinetic energy, and multiply the grid frequency rate of change by the corresponding inertia control coefficient, which is defined as (34),

$$\Delta P = \mathrm{M}_E \cdot d(\Delta f)/dt \tag{34}$$

Virtual inertia control can effectively prevent frequency changes, and the frequency change rate is superimposed on the electrolytic aluminum active output circuit such that the electrolytic aluminum system can react quickly according to the magnitude and direction of the grid frequency change rate.

C. INTEGRATED CONTROL STRATEGY

Droop control can make the load follow the grid frequency change quickly, and the virtual inertia control uses the grid frequency change rate to control the output to ensure that the electrolytic aluminum system can quickly respond and track the output according to the magnitude and direction of the grid frequency change rate. This effectively prevents incoming calls to the network frequency and further deterioration.

The two control methods can be reasonably switched to realize their complementary advantages and provide full frequency modulation ability. Virtual inertia control can effectively suppress the further grid frequency difference expansion. In the process of recovering from the maximum frequency difference to the steady state, the control strategy inhibits steady state recovery, which leads to a longer recovery time. Drop control has difficulty effectively changing the power grid frequency difference at the initial stage but can quickly restore the steady state during recovery.

The frequency modulation of the power grid was divided as degraded stage and restored stage. In the degraded stage, the virtual inertia control was adopted to control the system. In the restored stage, droop and virtual inertia control were combined to control the system. FIGURE 4 shows the integrated control strategy.

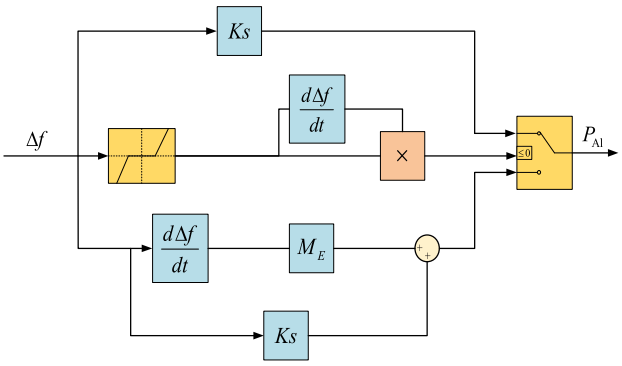

FIGURE 4. Coordinated integrated droop control and VSG control strategy.

V. SIMULATION ANALYSIS

A. COMPARISON OF CONTROL STRATEGIES

In this study, a two-region LFC model was built with a 0.01 perturbation added to region *i*. The traditional PID controller and the fractional PID controller effects designed in this study were compared to simulation. The conventional frequency modulation unit was a thermal power unit with a

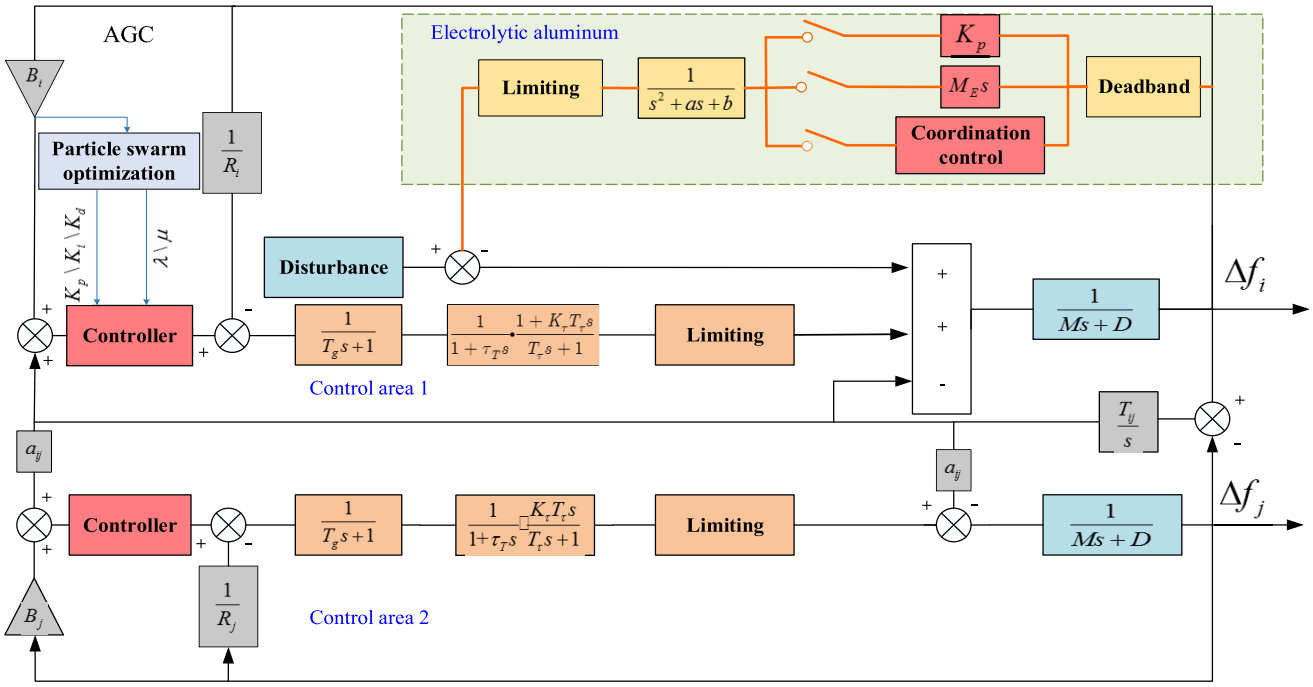

FIGURE 5. Typical automatic generation control framework.

rated power of 1000 MW. The specific unit parameters are listed in Table 1 [15]. The typical automatic generation control framework is shown in FIGURE 5. The particle swarm optimization (PSO) algorithm is used to optimize the fractional PID controller parameters, and the controller parameters are shown in Table 2 through 20 PSO iterations [18]. The simulation results are shown in FIGURE 6 and FIGURE 7.

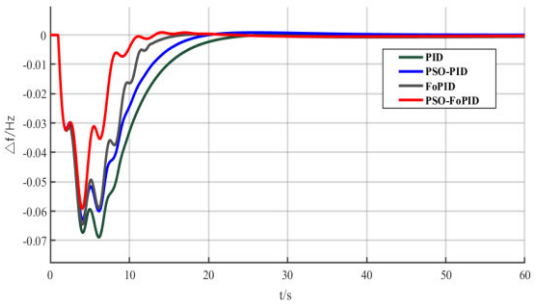

FIGURE 6. Comparison of control effect between traditional PID controller and fractional PID controller.

TABLE 1. Generator parameters.

Parameter	τ_T	T_τ	K_τ	T_g
Value	0.3	10	*0.5*	0.08

It can be seen from the simulation results of the above figure that the control effect of the fractional-order PID controller is significantly better than that of the traditional PID

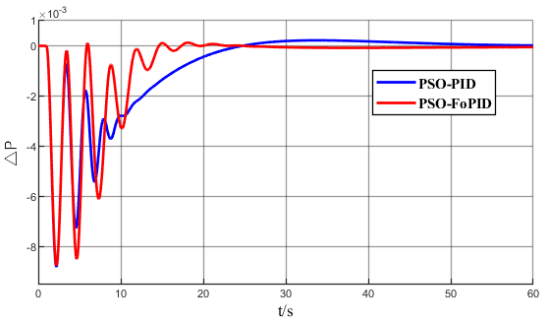

FIGURE 7. Tie line power under different controllers.

TABLE 2. Controller parameters.

	Parameter	Value	Parameters	Value
traditional PID	K_p	0.503	K_i	0.183
	K_d	0.271		
FOPID	K_p	54.0644	K_i	14.5721
	K_d	15.2911		
	μ	1.7286	λ	0.9191

controller. Facing the disturbance of 0.01, using the traditional PID controller, the rise time of the system is about 18s, while using the fractional PID controller, the rise time of the system is about 14s; using the fractional PID control, the rise time of the system is reduced by 28.5 %. From the perspective

of the maximum frequency deviation, the maximum deviation of the system frequency of the traditional PID are 0.0629; while the maximum deviation of the system frequency of the fractional PID are 0.0517, the frequency deviation from the system has been reduced. Therefore, the fractional PID control makes the system fast and stable, and the frequency deviation value is also reduced. The control effect of the system is better than the traditional PID control.

B. SIMULATION ANALYSIS OF ELECTROLYTIC ALUMINUM LOAD PARTICIPATING IN FREQUENCY MODULATION

1) COMPARISON OF DIFFERENT CONTROL STRATEGIES FOR ELECTROLYTIC ALUMINUM LOADING

This study simulated analysis of a 117 MW electrolytic aluminum load. At 2 s, a disturbance signal of 0.01 *pu* was applied in the form of a step signal in area *i* to imitate a sudden load increase. FIGURE 8 compares the frequency change after the electrolytic aluminum load participated in frequency modulation with different control methods. FIGURE 9 shows the electrolytic aluminum load output under different control strategies.

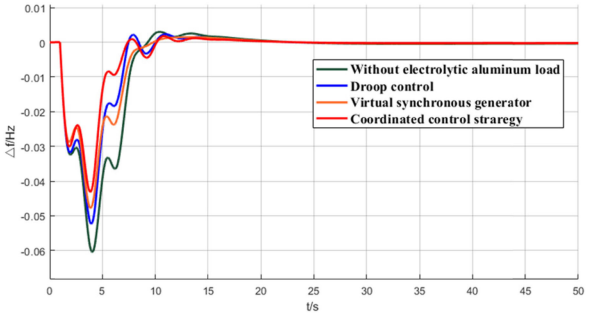

FIGURE 8. Comprehensive control strategy of electrolytic aluminum.

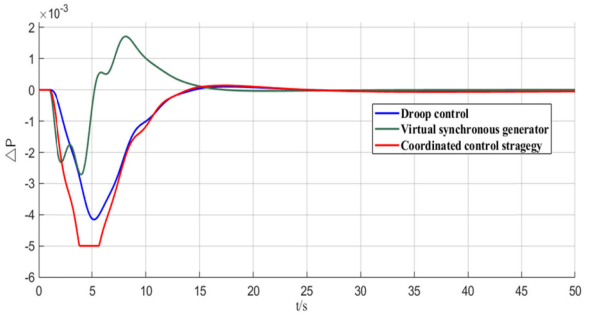

FIGURE 9. Output of electrolytic aluminum under integrated control strategy.

FIGURE 8 and FIGURE 9 shows that the electrolytic aluminum load effectively improved the grid frequency fluctuation under droop control, but the initial grid frequency difference improvement was poor, while the virtual inertia control quickly smoothed the initial frequency change. The grid frequency difference effectively prevented the grid frequency from deteriorating. In contrast, the recovery time under droop control mode was better than virtual inertia control. Under the integrated control strategy, the grid frequency fluctuation difference was smaller than that under any single control mode. To achieve a similar control effect for the electrolytic aluminum load output, the adjustable electrolytic aluminum load capacity involved in virtual inertia control is less than that involved in droop control, which meant that virtual inertia control reduced the electrolytic aluminum load. The capacity was involved in frequency modulation, and when virtual inertia was used, the electrolytic aluminum load frequency modulation efficiency was higher. Comparing the electrolytic aluminum output under the comprehensive control strategy, the adjustable capacity could be fully utilized, and the output reached the limit. Thus, the electrolytic aluminum load fully participated in the power grid frequency regulation.

2) DEMAND RESPONSE

The demand response load can be regarded as a set of spare capacities, which can be adjusted in real time according to the active power balance. Adjusting the active power balance adjusts power system frequency [11], [12]. Different from traditional ''power dispatching'', demand response uses schedulable resources on the demand side as alternative resources on the supply side, allowing some schedulable loads to respond to power system frequency fluctuations and fundamentally solving frequency fluctuation problems. In the face of disturbance, it is not necessary to directly involve all adjustable electrolytic aluminum loads in frequency modulation.

This study performed simulation analysis and verified the 5%, 8% and 10% electrolytic aluminum loads involved in frequency modulation. The simulation results are shown in FIGURE 10.

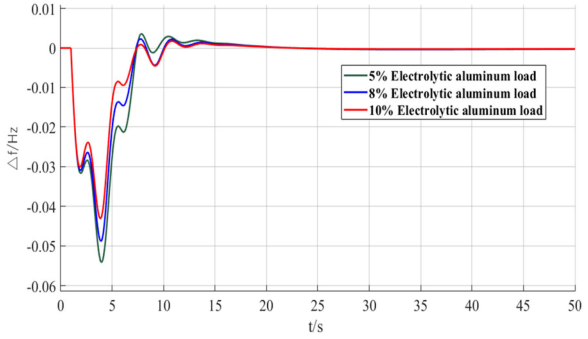

FIGURE 10. Demand response of electrolytic aluminum load.

From the simulation results, the frequency difference improvement effect of 5%, 8% and 10% electrolytic aluminum load participating in frequency modulation is gradually obvious. When 5% electrolytic aluminum loads participate, the maximum frequency difference is 5.46×10^{-2}Hz. When the aluminum load is involved, the maximum frequency difference is 4.357×10^{-2}Hz. It can be seen from the figure above that, when facing the same

disturbance, the electrolytic aluminum adjustable load participates in the frequency adjustment according to the demand of the power grid, which can effectively reduce the frequency fluctuation while reducing the adjustment time.

3) RANDOM DISTURBANCES

The influence of random factors was considered regarding unpredictable disturbances. Different perturbations were therefore set up to test the actual alumina load performance when it participated in grid frequency regulation. The effect of smoothing the grid frequency of a high energy-consuming industrial grid in the presence of uncertain disturbances was investigated. The simulation time domain was 40 s. The perturbation amplitude was [−0.015 p.u., 0.015 p.u], which compared the grid frequency fluctuations with and without alumina load participation. The simulation results are shown in FIGURE 11. The amplitude was considerably smaller, and the fluctuation was reduced, after the electrolytic aluminum load was involved in FM, which had a better smoothing effect.

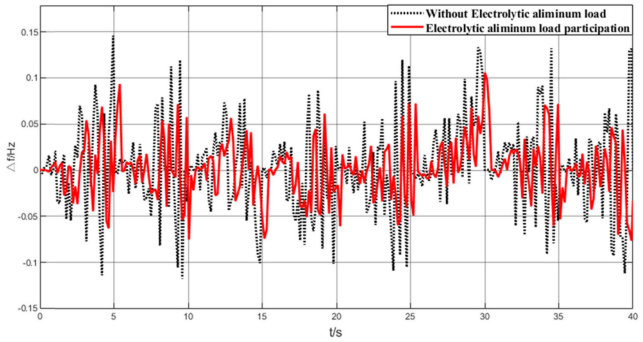

FIGURE 11. Frequency variation curves for random disturbances.

VI. CONCLUSION

In this paper, an integrated control strategy for electrolytic aluminum load to participate in the frequency modulation of the power grid based on the IEEE standard two-region LFC model is proposed. The integrated control strategy for electrolytic aluminum load participation in frequency modulation show that the FOPID controller optimized by the PSO algorithm has stronger robustness in the LFC. Different frequency control result with different demand response and random disturbance show that when the electrolytic aluminum load is used in the LFC, the frequency recovery time of the system was shortened and the dynamic performance of the secondary frequency regulation of the system was also improved.

REFERENCES

[1] N. Jaleeli and L. S. VanSlyck, "NERC's new control performance standards," *IEEE Trans. Power Syst.*, vol. 14, no. 3, pp. 1092–1099, Aug. 1999.
[2] I. Beil, I. Hiskens, and S. Backhaus, "Frequency regulation from commercial building HVAC demand response," *Proc. IEEE*, vol. 104, no. 4, pp. 745–757, Apr. 2016.
[3] P. Siano, "Demand response and smart grids-A survey," *Renew. Sustain. Energy Rev.*, vol. 30, no. 2, pp. 461–478, 2014.
[4] C. Zhao, U. Topcu, N. Li, and S. Low, "Design and stability of load-side primary frequency control in power systems," *IEEE Trans. Autom. Control*, vol. 59, no. 5, pp. 1177–1189, May 2014.
[5] T. Jiang, P. Ju, C. Wang, H. Li, and J. Liu, "Coordinated control of air-conditioning loads for system frequency regulation," *IEEE Trans. Smart Grid*, vol. 12, no. 1, pp. 548–560, Jan. 2021.
[6] H. Han, Q. Li, Z. Lv, and X. Yang, "Energy storage frequency response control considering battery aging of electric vehicle," in *Proc. IEEE Int. Conf. Energy Internet (ICEI)*, Apr. 2017, pp. 72–76.
[7] C. Chen, J. Wang, and S. Kishore, "A distributed direct load control approach for large-scale residential demand response," *IEEE Trans. Power Syst.*, vol. 29, no. 5, pp. 2219–2228, Sep. 2014.
[8] X. Zhang, G. Hug, J. Z. Kolter, and I. Harjunkoski, "Demand response of ancillary service from industrial loads coordinated with energy storage," *IEEE Trans. Power Syst.*, vol. 33, no. 1, pp. 951–961, Jan. 2018.
[9] J. Xu, S. Liao, Y. Sun, X.-Y. Ma, W. Gao, X. Li, J. Gu, J. Dong, and M. Zhou, "An isolated industrial power system driven by wind-coal power for aluminum productions: A case study of frequency control," *IEEE Trans. Power Syst.*, vol. 30, no. 1, pp. 471–483, Jan. 2015.
[10] S. Liao, J. Xu, Y. Sun, W. Gao, X.-Y. Ma, M. Zhou, Y. Qu, X. Li, J. Gu, and J. Dong, "Load-damping characteristic control method in an isolated power system with industrial voltage-sensitive load," *IEEE Trans. Power Syst.*, vol. 31, no. 2, pp. 1118–1128, Mar. 2016.
[11] T. Cui, W. Lin, Y. Sun, J. Xu, and H. Zhang, "Excitation voltage control for emergency frequency regulation of island power systems with voltage-dependent loads," *IEEE Trans. Power Syst.*, vol. 31, no. 2, pp. 1204–1217, Mar. 2016.
[12] Y. Bao, J. Xu, S. Liao, Y. Sun, X. Li, Y. Jiang, D. Ke, J. Yang, and X. Peng, "Field verification of frequency control by energy-intensive loads for isolated power systems with high penetration of wind power," *IEEE Trans. Power Syst.*, vol. 33, no. 6, pp. 6098–6108, Nov. 2018.
[13] H. Jiang, J. Lin, Y. Song, and D. J. Hill, "MPC-based frequency control with demand-side participation: A case study in an isolated wind-aluminum power system," *IEEE Trans. Power Syst.*, vol. 30, no. 6, pp. 3327–3337, Nov. 2015.
[14] E. A. Mohamed, E. M. Ahmed, A. Elmelegi, M. Aly, O. Elbaksawi, and A.-A.-A. Mohamed, "An optimized hybrid fractional order controller for frequency regulation in multi-area power systems," *IEEE Access*, vol. 8, pp. 213899–213915, 2020.
[15] K. Liu, J. He, Z. Luo, H. Shan, C. Li, R. Mei, Q. Yan, X. Wang, and L. Wei, "Load frequency control of pumped storage power station based on LADRC," *Processes*, vol. 8, no. 4, p. 380, Mar. 2020.
[16] H. Jiang, J. Lin, Y. Song, W. Gao, Y. Xu, B. Shu, X. Li, and J. Dong, "Demand side frequency control scheme in an isolated wind power system for industrial aluminum smelting production," *IEEE Trans. Power Syst.*, vol. 29, no. 2, pp. 844–853, Mar. 2014.
[17] Y. Bao, J. Xu, Y. Sun, X. Li, S. Liao, D. Ke, Y. Qu, and Y. Jiang, "An industrial verification of frequency regulation by electrolytic aluminum in an isolated power system," in *Proc. IEEE Power Energy Soc. Gen. Meeting (PESGM)*, Jul. 2016, pp. 1–5.
[18] F. Meng, S. Liu, A. Pang, and K. Liu, "Fractional order PID parameter tuning for solar collector system based on frequency domain analysis," *IEEE Access*, vol. 8, pp. 148980–148988, 2020.
[19] A. K. Barik and D. C. Das, "Expeditious frequency control of solar photovoltaic/biogas/biodiesel generator based isolated renewable microgrid using grasshopper optimisation algorithm," *IET Renew. Power Gener.*, vol. 12, no. 14, pp. 1659–1667, Oct. 2018.
[20] A. K. Barik, D. C. Das, and R. Muduli, "Demand response supported optimal load-frequency regulation of sustainable energy based four-interconnected unequal hybrid microgrids," in *Proc. IEEE Int. Conf. Sustain. Energy Technol. (ICSET)*, Feb. 2019, pp. 273–278.
[21] Z. Yan and Y. Xu, "A multi-agent deep reinforcement learning method for cooperative load frequency control of a multi-area power system," *IEEE Trans. Power Syst.*, vol. 35, no. 6, pp. 4599–4608, Nov. 2020.
[22] A. Latif, D. Chandra Das, A. K. Barik, and S. Ranjan, "Illustration of demand response supported co-ordinated system performance evaluation of YSGA optimized dual stage PIFOD-(1 + PI) controller employed with wind-tidal-biodiesel based independent two-area interconnected microgrid system," *IET Renew. Power Gener.*, vol. 14, no. 6, pp. 1074–1086, Apr. 2020.
[23] E. Vrettos, F. Oldewurtel, and G. Andersson, "Robust energy-constrained frequency reserves from aggregations of commercial buildings," *IEEE Trans. Power Syst.*, vol. 31, no. 6, pp. 4272–4285, Nov. 2016.

[24] A. K. Barik and D. C. Das, "Optimal load-frequency regulation of BioRenewable cogeneration based interconnected hybrid microgrids with demand response support," in *Proc. 15th IEEE India Council Int. Conf. (INDICON)*, Dec. 2018, pp. 1–6.
[25] K. Liu, J. He, Z. Luo, X. Shen, X. Liu, and T. Lu, "Secondary frequency control of isolated microgrid based on LADRC," *IEEE Access*, vol. 7, pp. 53454–53462, 2019.

XIN SHEN (Member, IEEE) was born in Qujing, Yunnan, China, in 1981. He received the B.Sc. and M.D. degrees from the Kunming University of Science and Technology, in 2003 and 2012, respectively, where he is currently pursuing the Ph.D. degree in automated transmission and transformation with the Department of Mechanical and Electrical Engineering.

HONGCHUN SHU (Member, IEEE) received the Ph.D. degree in electrical engineering from the Harbin Institute of Technology, Harbin, China, in 1997. He is currently a Professor and the Vice President of the Kunming University of Science and Technology, Kunming, China. His research interests include protective relay, fault location, and distribution networks. He is a Senior Member of the Chinese Society for Electrical Engineering.

ZHENGYUN FAN is currently with Yunnan Electric Power Supply Company, State Grid Electric Power Company. His research interest includes power system operation control.

XI MO is currently with the Yunnan Electric Power Dispatching and Control Center. His research interest includes power system operation control.